Spectral filtering modulation method for estimation of hemoglobin concentration and oxygenation based on a single fluorescence emission spectrum in tissue phantoms

Quan Liu[a)]
Division of Bioengineering, School of Chemical and Biomedical Engineering, Nanyang Technological University, Singapore 637457

Tuan Vo-Dinh[b)]
Fitzpatrick Institute for Photonics, Duke University, Durham, North Carolina 27708; Department of Biomedical Engineering, Duke University, Durham, North Carolina 27708; and Department of Chemistry, Duke University, Durham, North Carolina 27708

(Received 27 March 2009; revised 13 July 2009; accepted for publication 12 August 2009; published 25 September 2009)

Purpose: Hemoglobin concentration and oxygenation in tissue are important biomarkers that are useful in both research and clinical diagnostics of a wide variety of diseases such as cancer. The authors aim to develop simple ratiometric method based on the spectral filtering modulation (SFM) of fluorescence spectra to estimate the total hemoglobin concentration and oxygenation in tissue using only a single fluorescence emission spectrum, which will eliminate the need of diffuse reflectance measurements and prolonged data processing as required by most current methods, thus enabling rapid clinical measurements.

Methods: The proposed method consists of two steps. In the first step, the total hemoglobin concentration is determined by comparing a ratio of fluorescence intensities at two emission wavelengths to a calibration curve. The second step is to estimate oxygen saturation by comparing a double ratio that involves three emission wavelengths to another calibration curve that is a function of oxygen saturation for known total hemoglobin concentration. Theoretical derivation shows that the ratio in the first step is linearly proportional to the total hemoglobin concentrations and the double ratio in the second step is related to both total hemoglobin concentration and hemoglobin oxygenation for the chosen fiber-optic probe geometry. Experiments on synthetic fluorescent tissue phantoms, which included hemoglobin with both constant and varying oxygenation as the absorber, polystyrene spheres as scatterers, and flavin adenine dinucleotide as the fluorophore, were carried out to validate the theoretical prediction.

Results: Tissue phantom experiments confirm that the ratio in the first step is linearly proportional to the total hemoglobin concentration and the double ratio in the second step is related to both total hemoglobin concentrations and hemoglobin oxygenation. Furthermore, the relations between the two ratios and the total hemoglobin concentration and hemoglobin oxygenation are insensitive to the scattering property of the tissue model for the chosen probe geometry.

Conclusions: A simple two-step ratiometric method based on the SFM of fluorescence spectra is proposed to estimate the total hemoglobin concentration and oxygenation in a tissue model using only a single fluorescence emission spectrum. This method is immune to the variation in system throughput caused by inconsistent optical coupling because of its ratiometric nature. Calibration curves are insensitive to the scattering coefficient for the chosen probe geometry. Moreover, since only fluorescence intensities at a few wavelengths in a single fluorescence emission spectrum are needed in this method, the SFM method minimizes the amount of required data and reduces the data acquisition time. Finally, since this method does not use nonlinear regression, it can dramatically save computation time in data processing. The high sensitivity of the proposed method to superficial tissue volumes makes it ideal for fluorescence based oximetry and medical diagnostics in applications such as early epithelial cancer diagnosis or wherever the measured tissue volume is exposed to the outside such as in open surgery. [DOI: 10.1118/1.3218763]

Key words: hemoglobin concentration, hemoglobin oxygenation, oximetry, ratiometric, fluorescence spectroscopy

I. INTRODUCTION

Quantitative spectroscopic and imaging techniques for medical diagnostics have become a hot research area in the past decades. Hemoglobin concentration and oxygenation in tissue are important biomarkers that are useful in both research and clinical diagnostics of a wide variety of diseases such as

cancer. Several optical spectroscopy methods have been proposed to estimate these two parameters in tissue. These methods can be, in general, divided into four categories.

The first category of methods uses near-infrared (NIR) or resonance Raman spectroscopy, which include continuous-wave,[1–4] time-resolved,[5–7] or frequency-domain methods.[8,9] For example, Liu *et al.*[1] used continuous-wave NIR reflectance measurements measured at multiple source-detector separations (larger than 2 cm) to determine the optical properties and blood oxygenation in tissue. Svensson *et al.*[7] applied interstitial time-resolved NIR spectroscopy at three NIR wavelengths to the *in vivo* optical characterization of human prostate tissue. They estimated the total hemoglobin concentration and oxygen saturation from the derived absorption coefficients. Tromberg *et al.*[8] reviewed the use of frequency-domain photon migration in breast cancer diagnosis. By using a minimum of four NIR wavelengths, they were able to estimate the concentrations of four main absorbers in breast tissue, i.e., water, fat, oxy-, and deoxyhemoglobin, and correlated with the status of breast tissue. These methods use diffusion theory to model light transport in tissue, thus requiring large source-detector separations, which limit the spatial resolution of optical measurements. A NIR light source with at least two NIR wavelengths is required to estimate both hemoglobin concentration and oxygen saturation, which is usually large and expensive. Ward and co-workers[10,11] show that resonance Raman spectroscopy can be used to monitor the oxygenation of tissue vasculature. However, the weak Raman signal demands long data acquisition time, which limits its clinical applicability.

The second category of methods is based on diffuse reflectance spectroscopy in the visible spectrum,[12–14] in which Monte Carlo method or the analytical approximation to the transport equation is used to model light transport. Zonios *et al.*[14] used a modified diffusion theory to model diffuse reflectance with the concentrations of oxy- and deoxyhemoglobin and scattering properties as variables. The estimation of optical properties was carried out by performing a method of nonlinear regression such as the Gauss–Newton algorithm. Finlay and Foster[13,15] used the P_3 approximation of the transport equation to model forward light transport and the inversion was also done by nonlinear regression. Palmer *et al.*[12] used a scaling Monte Carlo method to create a diffuse reflectance database to enable rapid determination of diffuse reflectance detected by a fiber-optic probe geometry for the given optical properties and the inversions was done in a similar manner. The size of the fiber-optic probe used in the visible spectrum is significantly smaller. However, a broadband light source, such as a xenon or halogen lamp, is required for these methods thus the size of the equipment can be fairly large.

One common feature of the above two categories of methods is that they both measure diffusely scattered light from tissue at the same wavelength as the incident light. Such diffuse reflectance measurements gives rise to high signal to noise ratio but do not contain those diagnostic information that only fluorescence measurements can offer. Previous studies[16–18] in the optical diagnosis of breast cancer have shown that fluorescence measurements are complementary to diffuse reflectance measurements in terms of diagnostic information and the combination of both measurements will enhance the diagnostic accuracy. Unfortunately, a separate hardware module or separate measurement procedures have to be added for any of the above methods to enable fluorescence measurements, which would either add additional weight and cost to the equipment or prolong data acquisition time.

The third category of methods directly model fluorescence light propagation and fit fluorescence measurements to the model to estimate hemoglobin parameters and fluorescence parameters simultaneously.[12,13,19] Finlay *et al.*[13] created a forward-adjoint model based on a scaled Monte Carlo method to recover intrinsic fluorescence spectra and hemoglobin oxygen saturation in turbid samples and demonstrated its effectiveness in both phantom experiments and murine tumors *in vivo*. Cerussi*et al.*[19] presented a fluorescence photon migration model and experimentally demonstrated its capability with a frequency domain equipment to quantitatively recover the fluorescence spectral property in a homogeneous multiple-scattering fluorescence tissue phantom. Later, this model was used to recover the absorption, scattering, and fluorescence parameters in highly scattering media from a single frequency measurement.[20] This category of methods uses only fluorescence measurements; however, fitting data to a model with many free parameters could cause difficulty in the convergence of regression and large uncertainty in the results thus may not be suitable for real time measurements.

The fourth category of methods uses the ratios of reflectance or fluorescence at special wavelengths to estimate hemoglobin oxygenation. Stratonnikov*et al.*[21] developed a ratiometric method to estimate blood oxygen saturation from diffuse reflectance spectra. Their method does not provide fluorescence information and requires a broadband light source that can increase the size of the equipment. Leisey*et al.*[22] used a simplistic model to quantify myoglobin saturation in the perfused heart from fluorescence intensity measured at two excitation wavelengths. Their method requires two excitation wavelengths; moreover, the method simply uses Beer's law to model both excitation and fluorescence light propagation, which may not be valid for actual tissue measurement. In addition, many groups have used ratio techniques to extract intrinsic fluorescence that is presumably free of the distortion induced by tissue turbidity. For example, Kramer and Pearlstein[23] used the ratio of cerebral cortical fluorescence measured at one isosbestic wavelength and reference fluorescence measured at another isosbestic wavelength to correct NADH fluorescence for vascular artifacts. Anidjar*et al.*[24] used the ratio of tissue fluorescence at two wavelengths for differentiating neoplastic lesions and normal bladder tissue. In addition, a number of groups[25–28] reported using the ratio of fluorescence and diffuse reflectance or the variants of the ratio to correct for the effect of tissue absorption and scattering and obtain intrinsic fluorescence (see Ref. 29 for a more comprehensive review about this technique). However, none of those papers realized that

the fact that the ratio of fluorescence intensities at certain wavelengths is related to tissue absorption can be used to extract tissue absorption properties.

We propose a ratiometric method based on the spectral filtering modulation (SFM) of fluorescence spectra for the estimation of hemoglobin concentration and oxygenation using only a single fluorescence emission spectrum. Because our method directly uses fluorescence data to obtain hemoglobin information, it does not require separate equipments or measurement procedures for diffuse reflectance and fluorescence measurements, which could dramatically reduce the size and cost of the equipment and data acquisition time as compared to the first two categories of methods summarized previously. In the proposed method, the absorption of the target species, i.e., hemoglobin, causes the SFM effect on the fluorescence spectrum contributed by the primary fluorophore. By taking advantage of the assumptions that a major fluorophore dominates the measured fluorescence spectrum and hemoglobin is the major absorber, which was not fully taken advantage of in the fourth category of methods above, this method does not need to fit the spectrum to complicated mathematical light transport model, thus eliminating the uncertainty problem associated with the regression procedure used in the third category of methods described previously. The ratiometric nature of this method makes it resistant to the variation in optical coupling. Simple calibration curves are established for estimating total hemoglobin concentration and oxygen saturation. It is found that these curves are insensitive to the scattering coefficient for the chosen probe geometry. These unique features are highly desirable in clinical measurements. The theory behind the ratiometric SFM method and the inherent assumptions are presented first. Then the results from phantom experiments are shown to demonstrate the efficacy of the method. Finally the advantages and limitations of this method are discussed. The high sensitivity of the proposed method to superficial tissue volumes makes it ideal for fluorescence based oximetry and medical diagnostics in applications such as early epithelial cancer diagnosis or wherever the measured tissue volume is exposed to outside such as in open surgery.

II. METHODS

II.A. Theory

In general, the measured fluorescence for a tissue model in Fig. 1 can be expressed as

$$F_{\text{Measured}}(X_{\text{exc}},X_{\text{emm}}) = \int_{\text{Whole tissue volume}}\int\int \Phi(X_{\text{exc}},r)\phi(r)C_f(r)G(r,X_{\text{emm}})dr, \quad (1)$$

where $\Phi(X_{\text{exc}},r)$ is the fluence rate value at r that indicates the probability of excitation photons reaching r when launched from X_{exc}, $\phi(r)$ and $C_f(r)$ are the fluorescence quantum yield and fluorophore concentration at r, and $G(r,X_{\text{emm}})$ is the escape function that indicates the probability of fluorescence photons generating from r that eventually reach X_{emm}.

FIG. 1. Semi-infinite tissue model with the excitation and emission fibers on the top surface. The light gray area is the tissue and the dark gray area represents the excitation volume, which is small when the absorption coefficient at the excitation wavelength is large. r is an arbitrary location inside the tissue model.

Let us assume that the tissue model, as shown Fig. 1, is homogeneous and contains hemoglobin as the major absorber and a single known major fluorophore. The quantum yield and concentration of the fluorophore are independent of r and can be written as two constants, ϕ and C_f, respectively. Then Eq. (1) can be simplified to

$$F_{\text{Measured}}(X_{\text{exc}},X_{\text{emm}}) = \phi C_f \int_{\text{Whole tissue volume}}\int\int \Phi(X_{\text{exc}},r)G(r,X_{\text{emm}})dr. \quad (2)$$

Consider a probe geometry in which the source and detector fibers collocate at the same spatial location, as shown in Fig. 2. The diameter of the fibers is assumed to be large compared to light penetration depth so that light distribution can be treated as varying with depth z only.

Then Eq. (2) can be rewritten as

$$F_{\text{Measured}}(X_{\text{exc}},X_{\text{emm}}) = \phi C_f \int_0^{+\infty} \Phi(z)G(z)dz, \quad (3)$$

where z is the depth.

For the probe geometry shown in Fig. 2, the fluence rate distribution can be approximated as the summation of two exponential functions,[30] i.e.,

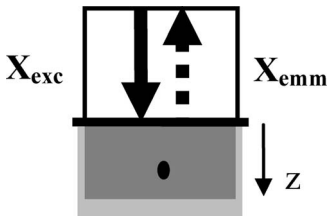

FIG. 2. Special excitation-emission geometry in which the source and detector fibers collocate at the same spatial location. The solid arrows indicate incident light rays, while the dashed arrows indicate emitted fluorescent light rays. The diameter of the fibers is assumed to be large compared to light penetration depth so that light distribution varies with depth only. The light gray area is the tissue and the dark gray area represents the excitation volume, whose axial dimension is small when the absorption at the excitation wavelength is high. The black dot in the gray area indicates the location of fluorescence origination.

TABLE I. Values of k_1, k_2, and k_3 for various diffuse reflectance values (i.e., R) and $n_{tissue}/n_{air}=1.33$.

R	k_1	k_2	k_3
10^{-2}	0.65	1.64	0.72
10^{-3}	0.59	1.60	0.70
10^{-4}	0.58	1.59	0.70
10^{-5}	0.58	1.59	0.70
10^{-6}	0.58	1.59	0.70

$$\Phi(z) = E_0(C_1 e^{-k_1 z/\delta_x} - C_2 e^{-k_2 z/\delta_x}). \quad (4)$$

Similarly, the escape function of fluorescence can also be expressed as an exponential function of the depth with a different attenuation constant,[30] i.e.,

$$G(z) = C_3 e^{-k_3 z/\delta_m}, \quad (5)$$

where E_0 is the incident light intensity, C_1, k_1, C_2, k_2, C_3, and k_3 are parameters that depend on diffuse reflectance, δ_x and δ_m are, respectively, the effective penetration depths at the excitation and emission wavelengths, which are defined as $\delta=1/\sqrt{3\mu_a[\mu_a+\mu_s(1-g)]}$ for the optical properties at the corresponding wavelength.

Let us assume that the excitation wavelength is close to the absorption peak of hemoglobin and that the emission wavelength is far away from the absorption peak. Then the absorption coefficient of the tissue model at the excitation wavelength is much greater than that at the emission wavelength, which leads to $\delta_x \ll \delta_m$ for typical tissue scattering coefficients and anisotropy factors. Because the values of k_1, k_2, and k_3 are similar as shown in Table I regardless of diffuse reflectance, the fluence rate function $\Phi(z)$ drops much faster with respect to z than the escape function $G(z)$, according to Eqs. (4) and (5). So in Eq. (3), the escape function $G(z)$ can be pulled out the integral and replaced with an averaged value, which is referred to as the effective escape value, i.e.,

$$F_{\text{Measured}}(X_{\text{exc}}, X_{\text{emm}}) = \phi C_f G_{\text{eff}} \int_0^{+\infty} \Phi(z)dz. \quad (6)$$

Consider the fluorescence intensity measured at two different emission wavelengths, λ_1 and λ_2, excited by the same excitation wavelength,

$$F_{\text{Measured\_1}} = \phi_1 C_f G_{\text{eff\_1}} \int_0^{+\infty} \Phi(z)dz \quad \text{at } \lambda_1, \quad (7)$$

$$F_{\text{Measured\_2}} = \phi_2 C_f G_{\text{eff\_2}} \int_0^{+\infty} \Phi(z)dz \quad \text{at } \lambda_2, \quad (8)$$

where the number in the subscript indicates the index of the emission wavelength.

Taking the ratio of Eqs. (7) and (8) yields

$$\frac{F_{\text{Measured\_1}}}{F_{\text{Measured\_2}}} = \frac{\phi_1}{\phi_2} \cdot \frac{G_{\text{eff\_1}}}{G_{\text{eff\_2}}}. \quad (9)$$

The original expression for G_{eff}, i.e., Eq. (5), contains a parameter k_3, which depends on the diffuse reflectance value at the emission wavelength and lacks intuitive physical meaning. So we modify the escape function as follows according to the Beer–Lambert law to elucidate the physical meanings of relevant parameters, i.e.,

$$G_{\text{eff}} = \int_0^{\infty} D(\mu_s, g, l) e^{-\mu_{a\_m} l} dl, \quad (10)$$

where l is the emission path length of fluorescent photons, D is the probability of a fluorescence photon being detected that depends on the scattering coefficient μ_s, the anisotropy factor g, and the emission path length l, and μ_{a_m} is the absorption coefficient at the emission wavelength. It should be noted that the emission path length l refers to the path length of a fluorescence photon from the location of fluorescence generation to the detector and does not include the path length from the incident location of excitation light to the location of fluorescence generation.

Incorporating Eq. (10) into Eq. (9) leads to

$$\frac{F_{\text{Measured\_1}}}{F_{\text{Measured\_2}}} = \frac{\phi_1}{\phi_2} \cdot \frac{\int_0^{\infty} D(\mu_{s\_1}, g_1, l) e^{-\mu_{a\_m1} l} dl}{\int_0^{\infty} D(\mu_{s\_2}, g_2, l) e^{-\mu_{a\_m2} l} dl}. \quad (11)$$

Assuming that two emission wavelengths are close to each other, the scattering coefficient and anisotropy factor at the two wavelengths can be considered approximately equal because it is known that the scattering coefficient of human tissue changes slowly with light wavelength, so $D(\mu_{s\_1}, g_1, l) \approx D(\mu_{s\_2}, g_2, l)$. Taking the natural log of Eq. (11) yields

$$\log\left(\frac{F_{\text{Measured\_1}}}{F_{\text{Measured\_2}}}\right) = \log\left(\frac{\phi_1}{\phi_2}\right) + \log\left(\frac{\int_0^{\infty} D(\mu_{s\_1}, g_1, l) e^{-\mu_{a\_m1} l} dl}{\int_0^{\infty} D(\mu_{s\_1}, g_1, l) e^{-\mu_{a\_m2} l} dl}\right). \quad (12)$$

The second term on the right side of Eq. (12) can be expanded in Taylor expansions[21] as follows:

$$\log\left(\frac{\int_0^{\infty} D(\mu_{s\_1}, g_1, l) e^{-\mu_{a\_m1} l} dl}{\int_0^{\infty} D(\mu_{s\_1}, g_1, l) e^{-\mu_{a\_m2} l} dl}\right) = -\langle l \rangle (\mu_{a\_m1} - \mu_{a\_m2}) + \frac{1}{2}\langle (l - \langle l \rangle)^2 \rangle (\mu_{a\_m1} - \mu_{a\_m2})^2 + o^3(\mu_{a\_m1} - \mu_{a\_m2}), \quad (13)$$

in which

$$\langle l \rangle = \frac{\int_0^{\infty} l \cdot D(\mu_{s\_1}, g_1, l) e^{-\mu_{a\_m1} l} dl}{\int_0^{\infty} D(\mu_{s\_1}, g_1, l) e^{-\mu_{a\_m1} l} dl},$$

$$\langle (l - \langle l \rangle)^2 \rangle = \frac{\int_0^{\infty} (l - \langle l \rangle)^2 \cdot D(\mu_{s\_1}, g_1, l) e^{-\mu_{a\_m1} l} dl}{\int_0^{\infty} D(\mu_{s\_1}, g_1, l) e^{-\mu_{a\_m1} l} dl},$$

and $o^3(\mu_{a\_m1} - \mu_{a\_m2})$ is the summation of the third and higher order polynomials. In other words, $\langle l \rangle$ is the emission path length averaged over the probability distribution of de-

tected fluorescence photons and $\langle(1-\langle l\rangle)^2\rangle$ is the variance. When the condition

$$\tfrac{1}{2}\langle(l-\langle l\rangle)^2\rangle \ll \langle l\rangle \tag{14}$$

is satisfied, Eq. (13) can be approximated in the first order, i.e.,

$$\log\left(\frac{\int_0^\infty D(\mu_{s\_1},g_1,l)e^{-\mu_{a\_m1}l}dl}{\int_0^\infty D(\mu_{s\_1},g_1,l)e^{-\mu_{a\_m2}l}dl}\right) \approx -\langle l\rangle(\mu_{a\_m1}-\mu_{a\_m2}). \tag{15}$$

Incorporating Eq. (14) into Eq. (12) yields

$$\log\left(\frac{F_{\text{Measured\_1}}}{F_{\text{Measured\_2}}}\right) \approx \log\left(\frac{\phi_1}{\phi_2}\right) - (\mu_{a\_m1}-\mu_{a\_m2})\langle l\rangle. \tag{16}$$

Because the absorption coefficient of the tissue model at the chosen excitation wavelength is large, the depth at which most fluorescent photons are generated is small, thus the range of possible path lengths is relatively narrow, which help meet the condition in Eq. (14).

Now two cases need to be considered separately for the estimation of hemoglobin concentration and oxygenation.

II.A.1. Hemoglobin with constant oxygenation

According to Beer–Lambert law, the absorption coefficient of a single absorber is proportional to its concentration, i.e.,

$$\mu_a = C_{\text{Hb}}\varepsilon_{\text{Hb}}, \tag{17}$$

where C_{Hb} is the concentration of hemoglobin with known oxygenation and ε_{Hb} is the molar extinction coefficient. Then Eq. (16) can be written as

$$\log\left(\frac{F_{\text{Measured\_1}}}{F_{\text{Measured\_2}}}\right) \approx \log\left(\frac{\phi_1}{\phi_2}\right) - C_{\text{Hb}}(\varepsilon_{\text{Hb\_1}}-\varepsilon_{\text{Hb\_2}})\langle l\rangle, \tag{18}$$

where $\varepsilon_{\text{Hb\_1}}$ and $\varepsilon_{\text{Hb\_2}}$ are, respectively, the molar extinction coefficients at λ_1 and λ_2.

According to Fig. 4 in Sec. III, $\langle l\rangle$ is a polynomial function of the absorption coefficient at the excitation wavelength so it is also a function of hemoglobin concentration. By assuming $\langle l\rangle = a + bC_{\text{Hb}} + cC_{\text{Hb}}^2$, Eq. (18) can be rewritten as

$$\log\left(\frac{F_{\text{Measured\_1}}}{F_{\text{Measured\_2}}}\right) \approx \log\left(\frac{\phi_1}{\phi_2}\right) - (aC_{\text{Hb}} + bC_{\text{Hb}}^2 + cC_{\text{Hb}}^3) \times(\varepsilon_{\text{Hb\_1}}-\varepsilon_{\text{Hb\_2}}). \tag{19}$$

When $b \ll a$ and $c \ll a$, Eq. (19) can be approximated as

$$\log\left(\frac{F_{\text{Measured\_1}}}{F_{\text{Measured\_2}}}\right) \approx \log\left(\frac{\phi_1}{\phi_2}\right) - aC_{\text{Hb}}(\varepsilon_{\text{Hb\_1}}-\varepsilon_{\text{Hb\_2}}). \tag{20}$$

The choices of λ_1 and λ_2 should maximize the difference in the extinction coefficient between two wavelengths for hemoglobin with constant oxygenation of interest; moreover, the fluorescence contributed by the tissue model at λ_1 and λ_2 needs to be strong compared to background fluorescence contributed by other nontissue factors. When flavin adenine dinucleotide (FAD) is the primary fluorophore and hemoglobin saturation is 100% or close to 100%, $\lambda_1 = 510$ nm and $\lambda_2 = 542$ nm would be a good choice of emission wavelengths because these two wavelengths are the local minimum and local maximum of oxyhemoglobin, respectively.

II.A.2. Hemoglobin with variable oxygenation

Let us assume that the total hemoglobin concentration is C_{tHb} and the that oxygen saturation is StO_2. The first step is to estimate the total hemoglobin concentration. Since the total absorption coefficient is contributed by both oxyhemoglobin (HbO_2) and deoxyhemoglobin (Hb), i.e.,

$$\mu_a = C_{\text{tHb}}(1-\text{StO}_2)\varepsilon_{\text{Hb}} + C_{\text{tHb}}\text{StO}_2\varepsilon_{\text{HbO}_2}, \tag{21}$$

the log of the ratio of measured fluorescence intensity at λ_1 and λ_2 in Eq. (16) becomes

$$\log\left(\frac{F_{\text{Measured\_1}}}{F_{\text{Measured\_2}}}\right) \approx \log\left(\frac{\phi_1}{\phi_2}\right) - [C_{\text{tHb}}(\varepsilon_{\text{Hb\_1}}-\varepsilon_{\text{Hb\_2}}) + C_{\text{tHb}}\text{StO}_2(\Delta\varepsilon_1-\Delta\varepsilon_2)]\langle l\rangle, \tag{22}$$

where $\Delta\varepsilon_1 = \varepsilon_{\text{HbO}_2\_1} - \varepsilon_{\text{Hb\_1}}$ and $\Delta\varepsilon_2 = \varepsilon_{\text{HbO}_2\_2} - \varepsilon_{\text{Hb\_2}}$.

If λ_1 and λ_2 are chosen at isosbestic wavelengths such that $\varepsilon_{\text{Hb\_1}} = \varepsilon_{\text{HbO}_2\_1}$ and $\varepsilon_{\text{Hb\_2}} = \varepsilon_{\text{HbO}_2\_2}$, then Eq. (22) will be reduced to

$$\log\left(\frac{F_{\text{Measured\_1}}}{F_{\text{Measured\_2}}}\right) \approx \log\left(\frac{\phi_1}{\phi_2}\right) - C_{\text{tHb}}(\varepsilon_{\text{Hb\_1}}-\varepsilon_{\text{Hb\_2}})\langle l\rangle, \tag{23}$$

which is essentially the same equation as Eq. (18) thus can be simplified to Eq. (20) for the probe geometry shown in Fig. 2.

In this study, the ratio of fluorescence intensity at 500 and 570 nm,

$$R_{\text{tHb}} = \frac{F_{500}}{F_{570}} \tag{24}$$

was used to estimate the concentration of the total hemoglobin. The extinction coefficients of oxygenated and deoxygenated hemoglobin at these two wavelengths are equal, as indicated by the circle symbols in Fig. 3.

In the second step, oxygen saturation is estimated by a double ratio that involves three emission wavelengths to enhance the sensitivity to oxygen saturation. According to Eq. (22), the double ratio can be expressed as

$$\log\left(\frac{F_{\text{Measured\_1}}}{F_{\text{Measured\_2}}}\cdot\frac{F_{\text{Measured\_3}}}{F_{\text{Measured\_2}}}\right) \approx \log\left(\frac{\phi_1}{\phi_2}\cdot\frac{\phi_3}{\phi_2}\right) - C_{\text{tHb}}[(\varepsilon_{\text{Hb\_1}}+\varepsilon_{\text{Hb\_3}}-2\varepsilon_{\text{Hb\_2}}) + \text{StO}_2(\Delta\varepsilon_1+\Delta\varepsilon_3-2\Delta\varepsilon_2)]\langle l\rangle, \tag{25}$$

where $\Delta\varepsilon_1 = \varepsilon_{\text{HbO}_2\_1} - \varepsilon_{\text{Hb\_1}}$, $\Delta\varepsilon_2 = \varepsilon_{\text{HbO}_2\_2} - \varepsilon_{\text{Hb\_2}}$, and $\Delta\varepsilon_3 = \varepsilon_{\text{HbO}_2\_3} - \varepsilon_{\text{Hb\_3}}$.

Equation (25) shows that the double ratio is related not only to StO_2 but also to C_{tHb}. It can be seen from Eq. (25) that maximizing $\Delta\varepsilon_1+\Delta\varepsilon_3-2\Delta\varepsilon_2$ will improve the sensitivity of the double ratio to StO_2. The star symbols in Fig. 3

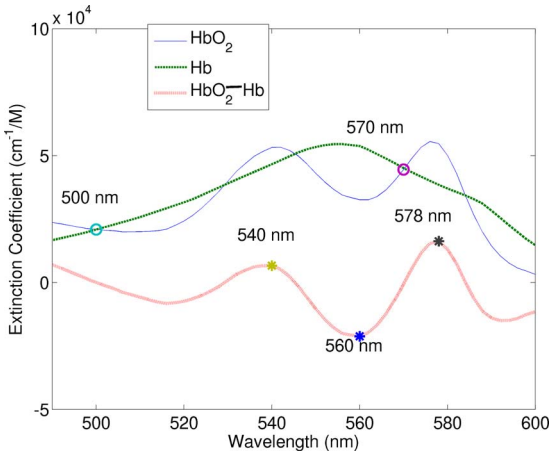

FIG. 3. Extinction coefficient spectra of oxy- and deoxyhemoglobin (adopted from http://omlc.ogi.edu/spectra/hemoglobin/). The dotted line is the difference in the extinction coefficient between two spectra. The circles represent two wavelengths (500 and 570 nm) for the estimation of the total hemoglobin concentration, while the stars represent three wavelengths (540, 560, and 578 nm) for the estimation of oxygen saturation.

illustrate the choice of the three emission wavelengths used in this study, which are $\lambda_1=540$ nm, $\lambda_2=560$ nm, and $\lambda_3=578$ nm. At 540 and 578 nm, the differences in the extinction coefficients between oxyhemoglobin and deoxyhemoglobin reach local maxima, while at 560 nm the difference reaches a minimum. Therefore, the double ratio, denoted by

$$R_{\mathrm{StO}_2}=\frac{F_{540}}{F_{560}}\cdot\frac{F_{578}}{F_{560}} \tag{26}$$

decreases with increasing oxygen saturation.

It is noted that Eq. (16) can be rewritten as

$$\frac{F_{\mathrm{Measured\_1}}}{F_{\mathrm{Measured\_2}}}\approx\frac{\phi_1}{\phi_2}\cdot e^{-(\mu_{a\_m1}-\mu_{a\_m2})\langle l\rangle}. \tag{27}$$

The exponent of the exponential term in Eq. (27) will be much smaller than 1 when hemoglobin concentration is low. Then to the first-order approximation of the exponential term, Eq. (27) can be written as

$$\frac{F_{\mathrm{Measured\_1}}}{F_{\mathrm{Measured\_2}}}\approx\frac{\phi_1}{\phi_2}\cdot[1-(\mu_{a\_m1}-\mu_{a\_m2})\langle l\rangle]. \tag{28}$$

All the subsequent derivations can be replaced by the corresponding first-order approximation. It turns out that the hemoglobin concentrations and probe geometry evaluated in this manuscript fall in this range. For this reason, the figures shown below are plotted on the linear scale rather than the log scale.

II.B. Synthetic fluorescent phantoms

The fluorescent phantoms used in this study contain three components, i.e., a fluorophore, an absorber, and scatterers. FAD (F6625, Sigma-Aldrich, St. Louis, MO) at a concentration of 24 μM were chosen as the fluorophore in the phantoms because of its biological importance in tissue diagnosis and its excellent solubility in water.

Hemoglobin (H0267, Sigma-Aldrich, St. Louis, MO), abbreviated as Hb, was used as the absorber. The absorption of Hb causes the SFM effect on the fluorescence spectra. The concentration of hemoglobin was varied from 7.8 to 46.5 μM, which corresponds to 3.5–21 cm^{-1} in the absorption coefficient at a wavelength of 414 nm to cover the absorption coefficient range of human tissue found in literature.[31] Polystyrene spheres (Polysciences, Inc., Warrington, PA) with 1-μm diameter were used as the scatterer and its volume concentration was adjusted to achieve a range of the scattering coefficient from 100 to 300 cm^{-1}. The phantoms were stored in a plastic vial, in which the volume height was about 3 cm and the diameter was 2 cm.

Two sets of phantoms were made to investigate both the case of constant oxygen saturation and the case of varying oxygen saturation. In the first set of phantoms, oxyhemoglobin was used as the absorber, whose oxygen saturation was 98%. Distilled water was used as the solvent. The concentration of oxyhemoglobin was varied from 7.8 to 46.5 μM with an increment of 7.8 μM. This set of phantoms was also used to establish the calibration curve for the estimation of total hemoglobin concentration, as shown in Fig. 6.

In the second set of phantoms, the concentration of hemoglobin was varied from 7.8 to 31 μM then to 46.5 μM. Phosphate buffer with a *p*H of 6.0 (phosphate buffer *p*H 6.0, 101410-742, VWR, Morrisville, NC) was used as the solvent in the phantoms with variable oxygenation to maintain a constant *p*H value, which keeps the relation between measured oxygen tension and hemoglobin oxygenation approximately unchanged when the temperature is fixed. The oxygen saturation was 98% at the beginning of optical measurements. Then the oxygen saturation of hemoglobin was varied by adding 1 mg/ml yeast (Rapid Rise Fleischmaqnn's Yeast, Chesterfield, MO) to remove oxygen from hemoglobin. The phantoms were consistently stirred at a moderate speed during measurements to maintain a uniform distribution of oxygenation. An oxygen electrode (MI-730, Microelectrodes, Inc., Bedford, NH) was used to monitor the change in oxygen pressure in the phantoms. The measured oxygen pressure was converted to hemoglobin saturation by Hill's equation with the required parameters such as *p*H and temperature measured by a *p*H meter (SympHony SB 70P, VWR, Morrisville, NC) and a multimeter (34XR-A, Amprobe, Everett, WA), respectively. It was found that the temperature and the *p*H of phantoms were maintained at approximately 22 °C and 5.95 throughout all measurements, respectively.

II.C. Instrumentation

A commercial fluorescence spectrophotometer (Fluomax-3, J.Y. Horiba Incorporated, Edison, NJ) was used to measure fluorescence spectra. The instrument incorporates a 150 W xenon lamp as the broadband white light source, a photomultiplier tube as the detector, and single excitation and single emission scanning monochromators for wavelength selection. The attached custom-made fiber-optic probe has a diameter of 3.78 mm and an effective numerical aperture of 0.22. The diameter of each individual fiber in the

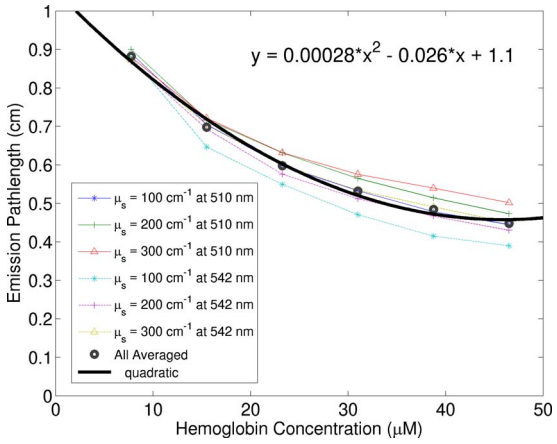

FIG. 4. Simulated average emission path length of fluorescence photons as a function of oxyhemoglobin concentration for various scattering coefficients. The two emission wavelengths used in the simulations, 510 and 542 nm, are the local minimum and maximum of oxyhemoglobin absorption spectrum. The absorption coefficients of deoxyhemoglobin for the wavelength range in this paper lie between the minimum and the maximum absorption coefficients of oxy-hemoglobin used in the simulations.

probe is 40 μm. The excitation and emission fibers in the probe are roughly equal numbered and randomly distributed across the common end of the probe, which is practically equivalent to a single large fiber for both excitation and emission.

III. RESULTS

Figure 4 shows simulated average emission path length, i.e., $\langle l \rangle$ in Eqs. (16), (18), and (23), of fluorescence photons as a function of oxyhemoglobin concentration for various scattering coefficients. A Monte Carlo code[32] was modified to record the emission path length of each individual fluorescence photon that escaped from the top surface of the tissue model. Then the emission path lengths of all detected fluorescence photons were averaged to generate the mean emission path length. As mentioned earlier, the probe for phantom measurements is practically equivalent to a single large fiber for both excitation and emission. Thus for simplicity, the simulations were performed for the probe geometry consisting of a single large fiber for both excitation and emission. From Fig. 4, it is clear that the average emission path length of detected photons is not sensitive to the scattering coefficient; moreover, the emission path length as a function of oxyhemoglobin concentration can be fitted by a quadratic function. Because the coefficients of the quadratic term and the linear term are much smaller than the constant term, the condition for Eq. (20) is satisfied, which infers that the ratio in Eq. (28) is approximately linearly related to the hemoglobin concentration.

Figure 5(a) shows the normalized fluorescence spectra for a range of oxygenated hemoglobin concentration, in which the oxygen saturation was kept as a constant (98%), when the scattering coefficient was varied from 100, 200, to 300 cm^{-1}. As hemoglobin concentration increases, the FAD fluorescence peak blueshifts, which is caused by the fact that

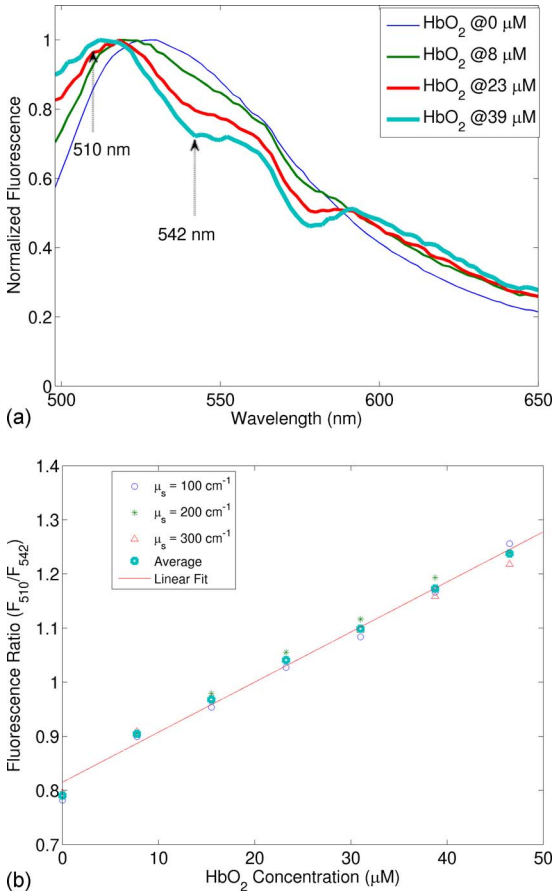

FIG. 5. (a) Fluorescence spectra for a range of oxygenated hemoglobin concentration from the first set of synthetic fluorescent phantoms, in which FAD was the fluorophore, 98% oxygenated hemoglobin (HbO_2) was the absorber, and the scattering coefficient was 200 cm^{-1}. Fluorescence spectra have been normalized by dividing each spectrum by its maximum fluorescence intensity for the wavelength range shown. The excitation wavelength was 414 nm. The dotted arrows indicate the two emission wavelengths (510 and 542 nm) chosen for the ratio calculation. (b) Ratio (F_{510}/F_{542}) as a function of HbO_2 concentration for scattering coefficients of 100, 200, and 300 cm^{-1}.

FAD fluorescence peak wavelength (around 528 nm) is located between the local minimum (510 nm) and the local maximum (542 nm) of oxyhemoglobin absorption spectrum. More importantly, when the total hemoglobin concentration increases, the normalized fluorescence intensity at 510 nm increases, while that at 542 nm decreases. This observation suggests that F_{510}/F_{542} would increase with oxyhemoglobin concentration, which was confirmed in Fig. 5(b). Figure 5(b) plots the fluorescence ratio (F_{510}/F_{542}) as a function of the concentration of oxyhemoglobin concentration. A linear relation clearly exists between the ratio and the concentration. Furthermore, this linear relation does not change with the scattering coefficient, which would provide significant convenience when applying this method to tissue measurements.

The ratio of F_{510}/F_{542} would not work for estimating the total hemoglobin concentration in the case of varying hemoglobin saturation. As suggested in Sec. II, another ratio $R_{\mathrm{tHb}}=F_{500}/F_{570}$ will work in this case. Figure 6 shows the ratio of fluorescence at two emission wavelengths ($R_{\mathrm{tHb}}=F_{500}/F_{570}$) as a function of the total hemoglobin concentra-

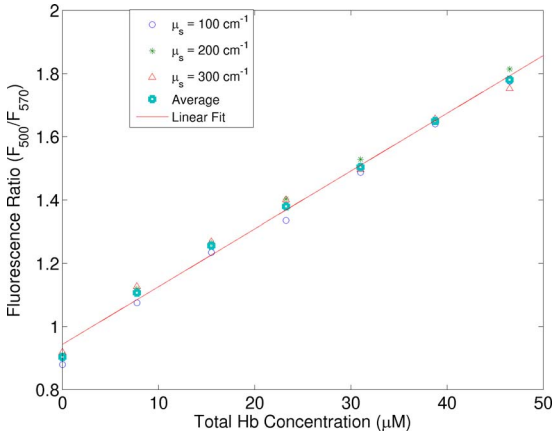

FIG. 6. Ratio of fluorescence at two emission wavelengths ($R_{tHb}=F_{500}/F_{570}$) as a function of the total hemoglobin concentration acquired from the first set of phantoms. The excitation wavelength was 414 nm. This figure can serve as the calibration curve for estimating the total hemoglobin concentration even hemoglobin oxygenation is different.

tion. Similar to Fig. 5(b), there exists a linear relation between the ratio and the total hemoglobin concentration and the relation is insensitive to the scattering coefficient. It should be pointed out that although the spectra were measured from the first set of phantoms, it can be used as the calibration curve for phantoms with different hemoglobin saturations because the extinction coefficients of oxy- and deoxyhemoglobin are equal at these two wavelengths.

Figure 7 shows the normalized fluorescence spectra for one of the second set of phantoms, in which oxygen saturation was varied by adding yeast to remove oxygen from hemoglobin, while the total hemoglobin concentration was fixed at 31 μM. Fluorescence spectra have been normalized by dividing each spectrum by the intensity at 560 nm as pointed by the middle arrow, at which the difference in the extinction coefficient between HbO_2 and Hb reaches a minimum. The other two arrows point to 540 and 578 nm, at which the differences in the extinction coefficients between HbO_2 and Hb reach local maxima. It can be seen that 540 and 578 nm are the two wavelengths that exhibit maximum differences in fluorescence spectra among various oxygen saturation, which confirms that $R_{StO_2}=F_{540}/F_{560}\cdot F_{578}/F_{560}$ is a good indicator of oxygen saturation as the theoretical derivation predicted.

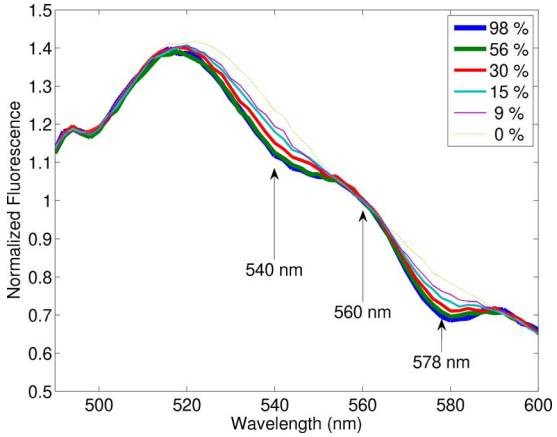

FIG. 7. Fluorescence spectra of one of the second set of phantoms with varying oxygen saturation of hemoglobin, in which the total hemoglobin concentration was fixed at 31 μM and the scattering coefficient was 200 cm^{-1}. The excitation wavelength was 414 nm. Fluorescence spectra were normalized by dividing each spectrum by the intensity at 560 nm as pointed by the middle arrow, at which the difference in the extinction coefficient between HbO_2 and Hb reaches a minimum. The other two arrows point to 540 and 578 nm, at which the differences in the extinction coefficients between HbO_2 and Hb reach local maxima, as shown in Fig. 3.

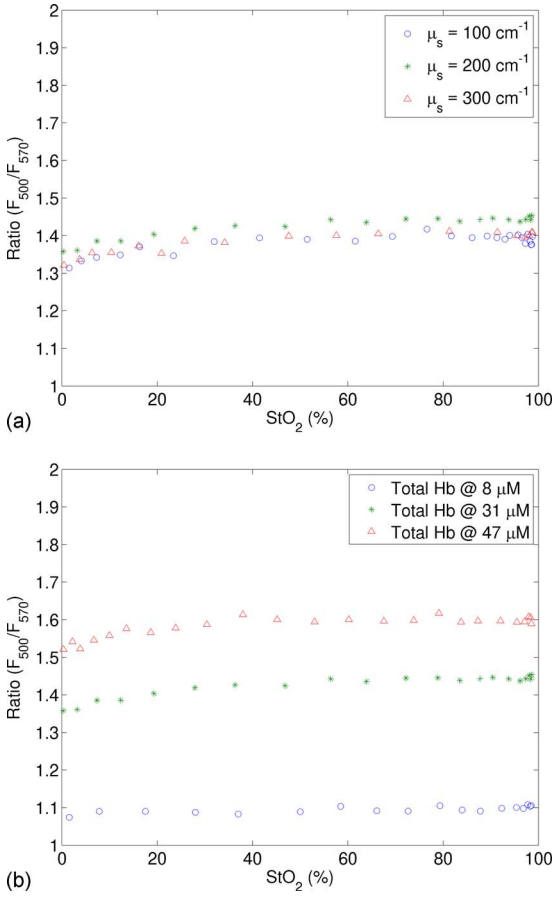

FIG. 8. Ratio of fluorescence intensities at two emission wavelengths ($R_{tHb}=F_{500}/F_{570}$) as a function of StO_2 (a) for varying scattering coefficient, while the total hemoglobin concentration was fixed at 31 μM and (b) for varying total hemoglobin concentration, while the scattering coefficient was fixed at 200 cm^{-1}. The excitation wavelength was 414 nm.

Figure 8(a) shows the ratio of fluorescence at two emission wavelengths ($R_{tHb}=F_{500}/F_{570}$) as a function of StO_2 for varying scattering coefficient, while the total hemoglobin concentration was fixed at 31 μM. It is clear that R_{tHb} remains approximately at a constant for all oxygen saturation values; moreover, this constant does not change with the scattering coefficient. Figure 8(b) displays similar data but for varying total hemoglobin concentration. Again, R_{tHb} remains approximately at a constant for a fixed total hemoglobin concentration but changes dramatically when the total hemoglobin concentration varies. This reinforces the observation in Fig. 7(a) that $R_{tHb}=F_{500}/F_{570}$ is a reliable indicator of the total hemoglobin concentration.

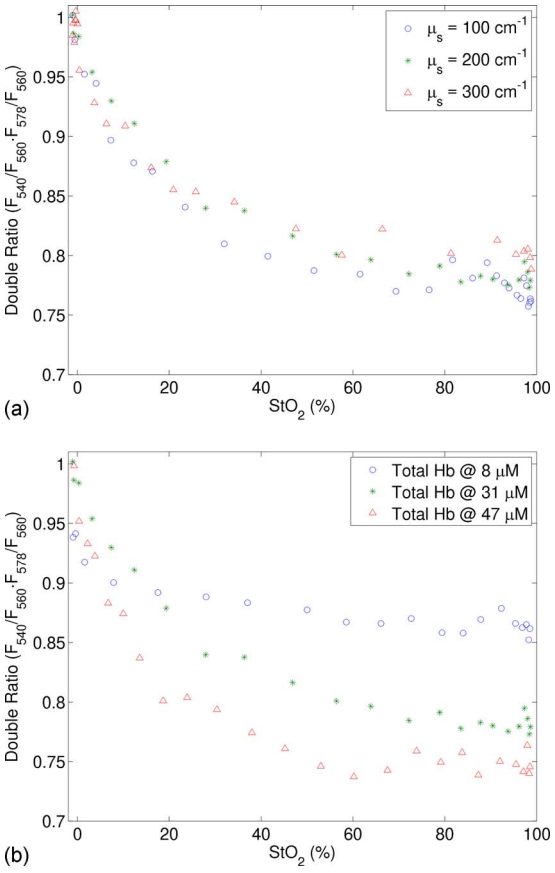

FIG. 9. Double ratio of fluorescence ($R_{StO_2}=F_{540}/F_{560}\cdot F_{578}/F_{560}$) as a function of StO_2 (a) for varying scattering coefficient, while the total hemoglobin concentration was fixed at 31 μM and (b) for varying total hemoglobin concentration, while the scattering coefficient was fixed at 200 cm^{-1}. The excitation wavelength was 414 nm.

Figure 9(a) shows the double ratio of fluorescence ($R_{StO_2}=F_{540}/F_{560}\cdot F_{578}/F_{560}$) as a function of StO_2 for varying scattering coefficient, while the total hemoglobin concentration was fixed at 31 μM. The double ratio monotonically decreases when oxygen saturation was increased from 0% to 98%. Furthermore, this relation is insensitive to the scattering coefficient. Figure 9(b) presents similar data for varying total hemoglobin concentration. As anticipated by Eq. (25), the double ratio is a function of both C_{tHb} and StO_2. More interestingly, the sensitivity of the double ratio to StO_2 increases with increasing C_{tHb}. This finding will be explained later in Sec. IV.

IV. DISCUSSION

The above results present a simple two-step ratiometric method for estimating total hemoglobin concentration and oxygen saturation based on a single fluorescence emission spectrum. Several advantages can be identified in this method for tissue measurements. First of all, because of its ratiometric nature, this method is immune to the variation in system throughput caused by inconsistent optical coupling. Secondly, only fluorescence intensities at a few wavelengths in a single fluorescence emission spectrum are needed in this method, which minimizes the amount of the required data. This will be a great advantage when this technique is transferred to an imaging setup. This technique can also be further developed to extract intrinsic fluorescence from measured raw fluorescence. Because this method only needs a single excitation wavelength and does not require separate diffuse reflectance measurements for absorption coefficient estimation, the size of the required equipment can be reduced significantly compared to many other methods for intrinsic fluorescence estimation. At last, this method does not use nonlinear regression as several other methods did,[12,13] which can dramatically save computation time in data processing. This feature is most desirable in real time imaging of hemoglobin information. In the following paragraphs, the inherent assumptions in the method and a few interesting findings in this study will be discussed.

One assumption in the derivation is the homogeneous distribution of hemoglobin in tissue, which may not be always true in the actual tissue. It should be noticed that the estimated hemoglobin concentration/saturation is actually the averaged contribution from the measured tissue volume. When the vessel size in the measured tissue volume (of the order of micrometers) is much smaller than the probed volume (in the order of mm), the potential effect of the inhomogenous distribution of blood vessels to optical measurements will be averaged out. When the vessel size is comparable to the probed volume, apparently optical measurements can be significantly altered. So the latter case should be avoided when applying our method to a tissue measurement.

In the derivation of Eq. (6), it is assumed that the absorption coefficient of the tissue model at the excitation is much greater than that at the emission wavelength. This assumption turns out to be important. The major absorption peak of oxyhemoglobin at 414 nm was chosen as the excitation wavelength for the data presented in this manuscript. Some other excitation wavelengths that are close to this peak such as 405 and 422 nm were also tried and found to work as well although not as good as 414 nm. However, an excitation wavelength such as 340 nm, which is far away from the absorption peak of hemoglobin, did not work in our experiment. It also should be pointed out that, since this method relies on tissue fluorescence measurements, fluorescence from the tissue model has to be much stronger than background fluorescence. Therefore special attention needs to be paid to achieve sufficiently strong fluorescence at the desired emission wavelengths from the tissue model at an excitation wavelength close to hemoglobin absorption peak.

Figure 8 shows that $R_{tHb}=F_{500}/F_{570}$ is a good indicator for the total hemoglobin concentration. Some other ratios, such as F_{529}/F_{545}, could be used for the same purpose. The ratio F_{529}/F_{545} as a function of StO_2 (results not shown) is flatter than $R_{tHb}=F_{500}/F_{570}$, which suggests that it is more insensitive to hemoglobin saturation and tissue scattering; but the sensitivity to the total hemoglobin concentration is lower. So the actual choices of wavelengths would be a trade-off between the insensitiveness to hemoglobin saturation and tissue scattering and the sensitivity to total hemoglobin concentration.

Figure 9(b) shows that the sensitivity of the double ratio $R_{StO_2}=F_{540}/F_{560}\cdot F_{578}/F_{560}$ to StO_2 increases with increasing C_{tHb}, which agrees with Eq. (25). It was noted in Eq. (25) that the double ratio is proportional to $C_{tHb}\cdot(\Delta\varepsilon_1+\Delta\varepsilon_3-2\Delta\varepsilon_2)\cdot\langle l\rangle\cdot StO_2$. Therefore the larger C_{tHb} is, the greater the double ratio will change when varying StO_2. When C_{tHb} is equal to or larger than 31 μM, the sensitivity of the double ratio to StO_2 is reasonably well for StO_2 smaller than 60%; however, when C_{tHb} is small or StO_2 is greater than 60%, the sensitivity of the double ratio to StO_2 is low. This is essentially determined by the nature of the ratio metric method. This method is based on fluorescence light absorption due to hemoglobin. Because only the emission path length plays a role in light absorption in this method, the sensitivity of the method to light absorption and, in turn, to hemoglobin concentration and oxygenation is lower than other methods using diffuse reflectance that takes advantage of the whole light path. Nevertheless, this limitation could be overcome to some extent by switching to other probe geometry that yields longer emission path length for detected fluorescence photons. Then calibration curves will need to be established for the new probe.

Yeast was used in this study to change the oxygen saturation of phantoms because the speed of deoxygenation can be adjusted by changing yeast concentration. It was noticed that yeast may slightly affect the optical properties of the phantoms and its effect could vary as yeast dissolves. This effect could contribute to the nonlinearity in the calibration curves for oxygen saturation.

The current method assumes a single fluorophore in the tissue model, which may not be practical in actual tissue measurements. The extension of the method to the case of multiple fluorophores and the extraction of intrinsic fluorescence that is free from the absorption effect of hemoglobin can be achieved by considering measured fluorescence as the summation of contribution from each individual fluorophore. We are also exploring to extend this method in an imaging setup for real time imaging of hemoglobin concentration and oxygenation.

Because of the shallow penetration depth of light at the peak absorption wavelength of hemoglobin, our method will be able to provide hemoglobin information in the superficial tissue volume, which can be very useful in many applications and early cancer diagnosis is one of these applications. Most cancers originate from the epithelium. Early cancers usually involve not only morphological changes in the epithelium, such as enlarged nuclei but also biochemical changes in the underlying stromal layer next to the epithelium, which is typically superficial (a few hundred of microns). The vascular alteration in the superficial stromal is an ideal clinical target of our method. So our method can be useful in the detection of early cancers. Another advantage of our method in clinical measurements is that superficial measurements also mean high sensitivity to the superficial changes in tissue. While other methods such as pulse oximetry can measure larger and deeper volumes, the sensitivity to changes in a small tissue volume is low because of the averaging effect of optical measurements.

V. CONCLUSION

We present a simple two-step ratiometric method based on the SFM of fluorescence spectra for estimating the total hemoglobin concentration and oxygen saturation based on a single fluorescence emission spectrum. In the first step, the ratio of fluorescence intensity at two emission wavelengths is used to estimate the total hemoglobin concentration by comparing it to a calibration curve. The second step is to estimate oxygen saturation by comparing a double ratio that involves three emission wavelengths to the second calibration curve that depends on oxygen saturation. Those calibration curves were found to be insensitive to the scattering property of the tissue model. Because our method directly uses fluorescence data to obtain hemoglobin information, it does not require separate equipments or measurement procedures for diffuse reflectance and fluorescence measurements, which could dramatically reduce the size and cost of the equipment and the data acquisition time for clinical measurements.

Several advantages in our method were identified that make it attractive in tissue measurements. First, our method is immune to the variation in the system throughput caused by inconsistent optical coupling because of its ratiometric nature. Second, only fluorescence intensities at a few wavelengths in a single fluorescence emission spectrum are needed in this method, which minimizes the amount of required data and potentially reduces the size of the required equipment. At last, the fact that this method does not use nonlinear regression can dramatically save computation time in data processing, which makes it possible to perform real time quantitative imaging of hemoglobin concentration and oxygen saturation. The proposed method in combination with fluorescence spectroscopy can be applied to fluorescence based oximetry and medical diagnostics in applications such as early cancer diagnosis in which hemoglobin information is important. The high sensitivity of the proposed method to superficial tissue volumes makes it ideal for fluorescence based oximetry and medical diagnostics in applications such as epithelial cancer diagnosis or wherever the measured tissue volume is exposed to outside such as in open surgery.

ACKNOWLEDGMENT

The authors acknowledge financial support from the National Institutes of Health (Grant No. R01 CA088787).

[a]Electronic mail: quanliu@ntu.edu.sg
[b]Author to whom correspondence should be addressed. Electronic mail: tuan.vodinh@duke.edu

[1]H. Liu, D. A. Boas, Y. Zhang, A. G. Yodh, and B. Chance, "Determination of optical properties and blood oxygenation in tissue using continuous NIR light," Phys. Med. Biol. **40**, 1983–1993 (1995).
[2]R. P. Kennan and K. L. Behar, "Continuous-wave near-infrared spectroscopy using pathlength-independent hypoxia normalization," J. Biomed. Opt. **7**, 228–235 (2002).
[3]G. A. Breit, J. H. Gross, D. E. Watenpaugh, B. Chance, and A. R. Har-

gens, "Near-infrared spectroscopy for monitoring of tissue oxygenation of exercising skeletal muscle in a chronic compartment syndrome model," J. Bone Jt. Surg., Am. Vol. Vol. **79**, 838–843 (1997).
[4]D. E. Myers, L. D. Anderson, R. P. Seifert, J. P. Ortner, C. E. Cooper, G. J. Beilman, and J. D. Mowlem, "Noninvasive method for measuring local hemoglobin oxygen saturation in tissue using wide gap second derivative near-infrared spectroscopy," J. Biomed. Opt. **10**, 034017-1–034017-18 (2005).
[5]T. Hamaoka, T. Katsumura, N. Murase, S. Nishio, T. Osada, T. Sako, H. Higuchi, Y. Kurosawa, T. Shimomitsu, M. Miwa, and B. Chance, "Quantification of ischemic muscle deoxygenation by near infrared time-resolved spectroscopy," J. Biomed. Opt. **5**, 102–105 (2000).
[6]H. Liu, B. Chance, A. H. Hielscher, S. L. Jacques, and F. K. Tittel, "Influence of blood vessels on the measurement of hemoglobin oxygenation as determined by time-resolved reflectance spectroscopy," Med. Phys. **22**, 1209–1217 (1995).
[7]T. Svensson, S. Andersson-Engels, M. Einarsdottir, and K. Svanberg, "In vivo optical characterization of human prostate tissue using near-infrared time-resolved spectroscopy," J. Biomed. Opt. **12**, 14022–14021 (2007).
[8]B. J. Tromberg, N. Shah, R. Lanning, A. Cerussi, J. Espinoza, T. Pham, L. Svaasand, and J. Butler, "Non-invasive in vivo characterization of breast tumors using photon migration spectroscopy," Neoplasia **2**, 26–40 (2000).
[9]J. B. Fishkin, O. Coquoz, E. R. Anderson, M. Brenner, and B. J. Tromberg, "Frequency-domain photon migration measurements of normal and malignant tissue optical properties in a human subject," Appl. Opt. **36**, 10–20 (1997).
[10]K. R. Ward, R. W. Barbee, P. S. Reynolds, I. P. Torres, M. H. Tiba, L. Torres, R. N. Pittman, and J. Terner, "Oxygenation monitoring of tissue vasculature by resonance Raman spectroscopy," Anal. Chem. **79**, 1514–1518 (2007).
[11]K. R. Ward, I. Torres Filho, R. W. Barbee, L. Torres, M. H. Tiba, P. S. Reynolds, R. N. Pittman, R. R. Ivatury, and J. Terner, "Resonance Raman spectroscopy: A new technology for tissue oxygenation monitoring," Crit. Care Med. **34**, 792–799 (2006).
[12]G. M. Palmer and N. Ramanujam, "Monte Carlo-based inverse model for calculating tissue optical properties. Part I. Theory and validation on synthetic phantoms," Appl. Opt. **45**, 1062–1071 (2006).
[13]J. C. Finlay and T. H. Foster, "Recovery of hemoglobin oxygen saturation and intrinsic fluorescence with a forward-adjoint model," Appl. Opt. **44**, 1917–1933 (2005).
[14]G. Zonios, L. T. Perelman, V. Backman, R. Manoharan, M. Fitzmaurice, J. Van Dam, and M. S. Feld, "Diffuse reflectance spectroscopy of human adenomatous colon polyps in vivo," Appl. Opt. **38**, 6628–6637 (1999).
[15]J. C. Finlay and T. H. Foster, "Hemoglobin oxygen saturations in phantoms and in vivo from measurements of steady-state diffuse reflectance at a single, short source-detector separation," Med. Phys. **31**, 1949–1959 (2004).
[16]G. M. Palmer, C. Zhu, T. M. Breslin, F. Xu, K. W. Gilchrist, and N. Ramanujam, "Comparison of multiexcitation fluorescence and diffuse reflectance spectroscopy for the diagnosis of breast cancer (March 2003)," IEEE Trans. Biomed. Eng. **50**, 1233–1242 (2003).
[17]Z. Volynskaya, A. S. Haka, K. L. Bechtel, M. Fitzmaurice, R. Shenk, N. Wang, J. Nazemi, R. R. Dasari, and M. S. Feld, "Diagnosing breast cancer using diffuse reflectance spectroscopy and intrinsic fluorescence spectroscopy," J. Biomed. Opt. **13**, 024012-1–024012-9 (2008).
[18]C. Zhu, G. M. Palmer, T. M. Breslin, J. Harter, and N. Ramanujam, "Diagnosis of breast cancer using fluorescence and diffuse reflectance spectroscopy: A Monte-Carlo-model-based approach," J. Biomed. Opt. **13**, 034015-1–034015-15 (2008).
[19]A. E. Cerussi, J. S. Maier, S. Fantini, M. A. Franceschini, W. W. Mantulin, and E. Gratton, "Experimental verification of a theory for the time-resolved fluorescence spectroscopy of thick tissues," Appl. Opt. **36**, 116–124 (1997).
[20]J. S. Maier, A. E. Cerussi, S. Fantini, and E. Gratton, "Experimental recovery of absorption, scattering, and fluorescence parameters in highly-scattering media from a single frequency measurement," Proc. SPIE **2979**, 6–13 (1997).
[21]A. A. Stratonnikov and V. B. Loschenov, "Evaluation of blood oxygen saturation in vivo from diffuse reflectance spectra," J. Biomed. Opt. **6**, 457–467 (2001).
[22]J. R. Leisey, D. A. Scott, L. W. Grotyohann, and R. C. Scaduto, "Quantitation of myoglobin saturation in the perfused heart using myoglobin as an optical inner filter," Am. J. Physiol. **267**, H645–H653 (1994).
[23]R. S. Kramer and R. D. Pearlstein, "Cerebral cortical microfluorometry at isosbestic wavelengths for correction of vascular artifact," Science **205**, 693–696 (1979).
[24]M. Anidjar, O. Cussenot, S. Avrillier, D. Ettori, P. Teillac, and A. Le Duc, "The role of laser-induced autofluorescence spectroscopy in bladder tumor detection. Dependence on the excitation wavelength," Ann. N.Y. Acad. Sci. **838**, 130–142 (1998).
[25]N. C. Biswal, S. Gupta, N. Ghosh, and A. Pradhan, "Recovery of turbidity free fluorescence from measured fluorescence: An experimental approach," Opt. Express **11**, 3320–3331 (2003).
[26]J. C. Finlay, D. L. Conover, E. L. Hull, and T. H. Foster, "Porphyrin bleaching and PDT-induced spectral changes are irradiance dependent in ALA-sensitized normal rat skin in vivo," Photochem. Photobiol. **73**, 54–63 (2001).
[27]M. G. Muller, I. Georgakoudi, Z. Qingguo, W. Jun, and M. S. Feld, "Intrinsic fluorescence spectroscopy in turbid media: Disentangling effects of scattering and absorption," Appl. Opt. **40**, 4633–4646 (2001).
[28]J. Y. Qu and H. Jianwen, "Calibrated fluorescence imaging of tissue in vivo," Appl. Phys. Lett. **78**, 4040–4042 (2001).
[29]R. S. Bradley and M. S. Thorniley, "A review of attenuation correction techniques for tissue fluorescence," J. R. Soc., Interface **3**, 1–13 (2006).
[30]C. M. Gardner, S. L. Jacques, and A. J. Welch, "Light transport in tissue: Accurate expressions for one-dimensional fluence rate and escape function based upon monte carlo simulation," Lasers Surg. Med. **18**, 129–138 (1996).
[31]R. Drezek, K. Sokolov, U. Utzinger, I. Boiko, A. Malpica, M. Follen, and R. Richards-Kortum, "Understanding the contributions of NADH and collagen to cervical tissue fluorescence spectra: Modeling, measurements, and implications," J. Biomed. Opt. **6**, 385–396 (2001).
[32]Q. Liu, C. Zhu, and N. Ramanujam, "Experimental validation of Monte Carlo modeling of fluorescence in tissues in the UV-visible spectrum," J. Biomed. Opt. **8**, 223–236 (2003).